FIGURE S1

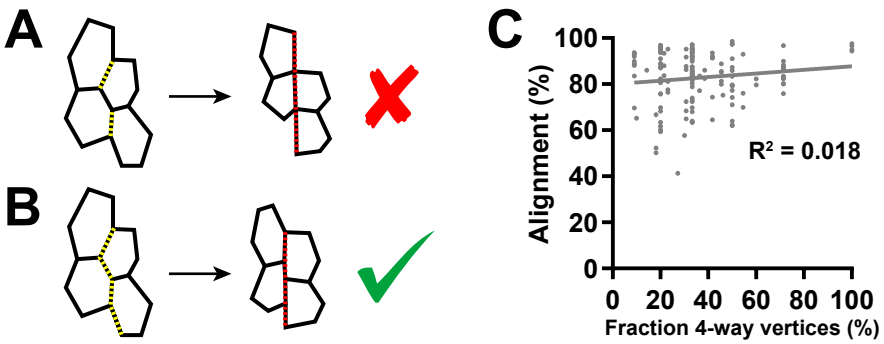

Figure S1. Alignment is driven by coordinated cell shape changes rather than junction remodeling.

(A and B) Two models can explain the alignment morphology. (A) The first involves elevated contractility along select junctions in the interface driving remodeling events to create 4-way vertices. (B) The second model has cortical tension elevated along all contacts of the interface to drive coordinated cell shape changes. Yellow dashed lines indicate location of elevated tension.

(C) A lack of correlation between the presence of 4-way vertices and the alignment of the interface eliminated (A) the first model (see STAR Methods). The R^2 value from a Pearson correlation test is shown as well as a linear regression fit. N = 3 interfaces, 3 embryos

FIGURE S2

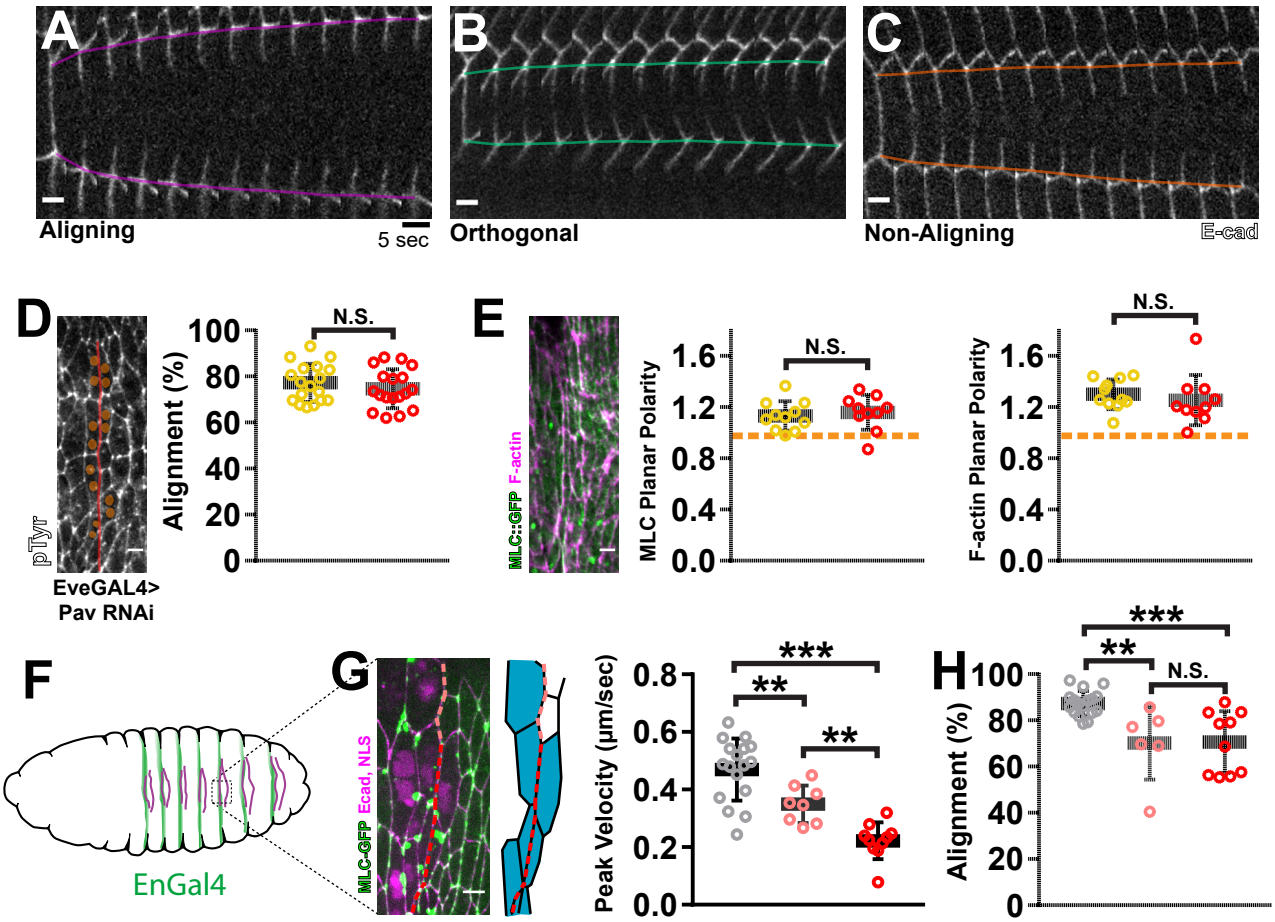

Figure S2. Local contractile force along interfaces drives collective cell shape changes during alignment.

(A-C) Representative montages of retraction in response to laser ablation for (A) aligning, (B) orthogonal and (C) non-aligning junctions. The first image in each sequence shows the junction prior to ablation and each subsequent frame represents a five second interval. Pseudo-colored lines map out the trajectory of motion for the vertices that connect the cut junction.

(D) Blocking cytokinesis by Pavarotti knockdown did not cause alignment defects. The position of nuclei in binucleated cells along the aligning interface were identified by Hoechst staining in deeper sections (not shown) and are marked in orange. In the graph, red shows alignment measurements of Eve-GAL4 > Pav RNAi interfaces while yellow are control, non-expressing interfaces. pTyr staining marked cell outlines. CTRL: 11 interfaces, 4 embryos; Pav RNAi: 12 interfaces, 4 embryos

(E) Pav knockdown also did not affect F-actin (magenta) or MLC (green) enrichment to aligning interfaces. CTRL: 11 interfaces, 4 embryos; Pav RNAi: 11 interfaces, 4 embryos

(F) A schematic of the Engrailed-GAL4 expression pattern (green) on the ventral face of the embryonic epithelium. Aligning interfaces are marked with purple lines. Only the anterior interface of each pair will be affected by Engrailed-GAL4.

(G) Engrailed-GAL4 variably expressed DeGradFP in cells at the anterior aligning interfaces. NLS-mCherry positively marked Engrailed-GAL4 expressing cells. Along the anterior aligning interface (dashed line), cells affected by DeGradFP-mediated MLC depletion are schematically shown in blue. Cells anterior (left) of the interface always expressed DeGradFP. Without expression on the posterior side (right), this resulted in unilateral knockdown (pink dashed lines and data points). Variably, Engrailed-GAL4 expressed DeGradFP in cells posterior to the interface, resulting in bilateral knockdown (red dashed lines and data points). Both cases resulted in decreased cortical tension compared to aligning junctions in wild-type rescue controls (gray). Bilateral knockdown caused a greater reduction in tension compared to unilateral knockdown. WT CTRL: junctions = 17 junctions from 6 embryos; Unilateral KD: 8 junctions from 6 embryos; Bilateral KD: 10 interfaces from 10 embryos)

(H) Alignment was equivalently defective in both unilateral and bilateral knockdown scenarios.

***$p<0.0001$, **$p<0.001$, Mann-Whitney U-test, Error bars = S.D. Scale bars = 4μm. Error bars = S.D.

FIGURE S3

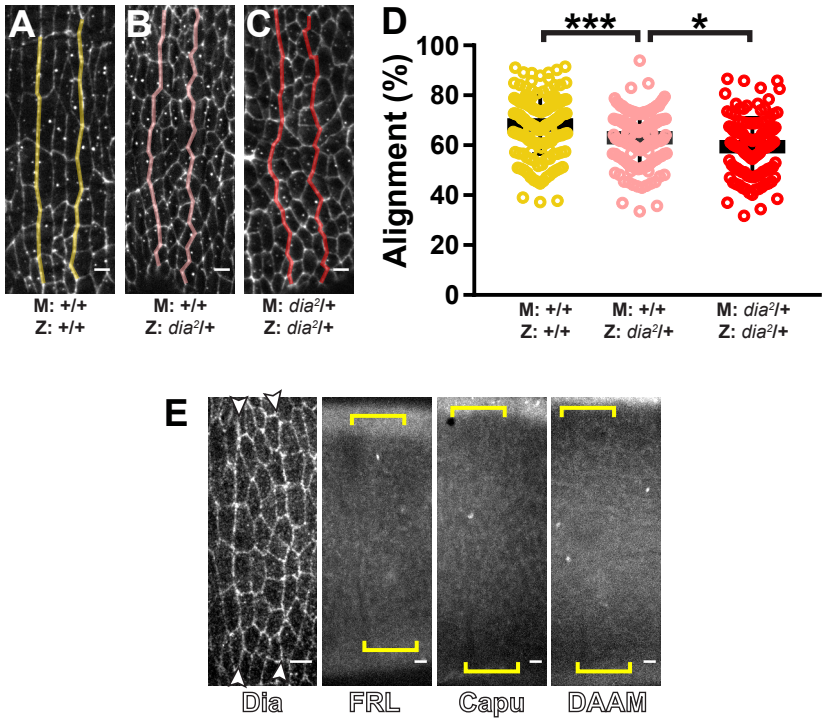

Figure S3. Diaphanous is the only formin involved in alignment.

(A-D) Partial genetic depletion of Dia causes alignment defects. (B) Embryos heterozygous for the null allele *dia*^{2} (pink) experience a partial depletion of their zygotically (Z) contributed Dia protein. (A) Relative to wild type controls (yellow), this zygotic reduction caused significant defects in alignment (D yellow vs pink). (C) Embryos laid by heterozygous females experience an additional depletion of maternally(M)-contributed Dia protein (red). Heterozygous embryos of this category had more severe defects in alignment compared to *dia*^{2} heterozygotes laid by wild type mothers (D, pink vs red). (A-C) pTyr staining was used to visualize cell outlines. A: interfaces = 157, 13 embryos; B: 137 interfaces, 10 embryos; C: 126 interfaces, 12 embryos

(E) We surveyed high-throughput sequencing data sets and *in situ* hybridization studies (flybase.org) of all formins in the Drosophila genome. Only three (FRL, Capu and DAAM), are expressed during the developmental stages relevant to alignment (FRL, Capu and DAAM). For each of these, we assessed the localization of endogenously GFP-tagged transgenic lines. These three formins showed homogeneous cytoplasmic distributions with little cortical targeting, compared to Dia (visualized by antibody staining). Yellow brackets indicate region of aligning interfaces. Dia antibody stain: Representative of 8 embryos; FRL::GFP: representative of 10 embryos; Capu::GFP: representative of 12 embryos; DAAM::GFP: representative of 13 embryos

***p<0.0001, *p<0.01, Mann-Whitney U-test, Error bars = S.D. Scale bars = 4μm.

FIGURE S4

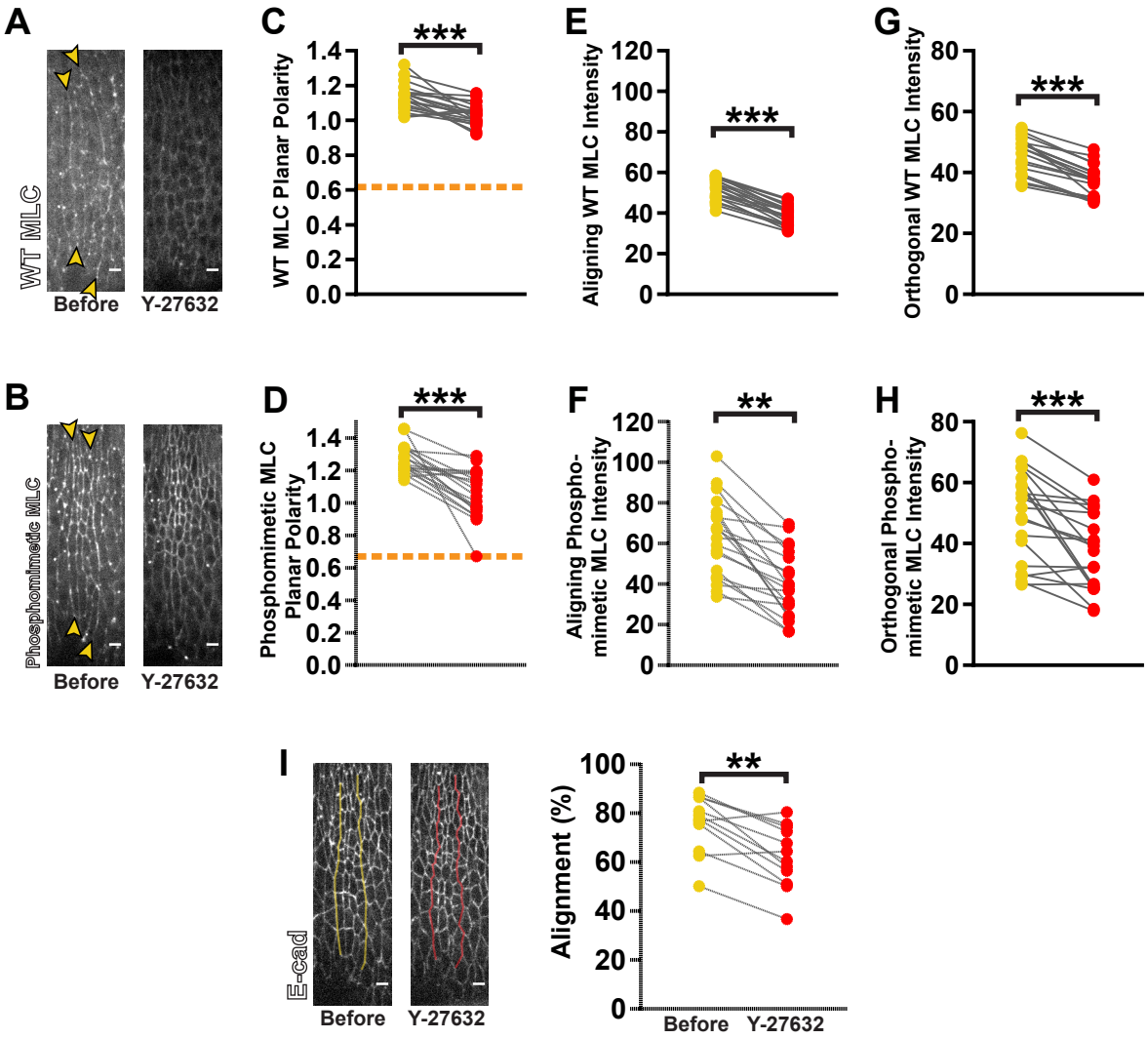

Figure S4. Phosphorylation is not sufficient for Myosin activity or polarity.

(A-H) Phosphorylation of MLC by ROK is not sufficient for junctional recruitment and planar polarity. (A) GFP-labelled wild type MLC or (B) phosphomimetic MLC were expressed with a similar transgenic strategy so that protein levels would not confound analysis. (C, D, yellow) Both versions of MLC were planar polarized properly to aligning interface. Upon ROK inhibition (red), both constructs lost (C, D) planar polarity and exhibited decreased cortical targeting to both (E, F) aligning junctions and (G,H) orthogonal junctions (G, H).

(I) Embryo expressing phosphomimetic MLC still exhibited significant alignment defects upon ROK inhibitor treatment. E-cadherin-tdTomato was used to visualize cell outlines.

sqh-sqh^{WT}::GFP: 20 interfaces from 5 embryos; sqh-sqh^{EE}::GFP: 20 interfaces from 6 embryos

Each lines in graphs represents one interface and matches measurements before and after drug treatment.

***p<0.0001, **p<0.01, Mann-Whitney U-test, Scale bars = 4μm.

FIGURE S5

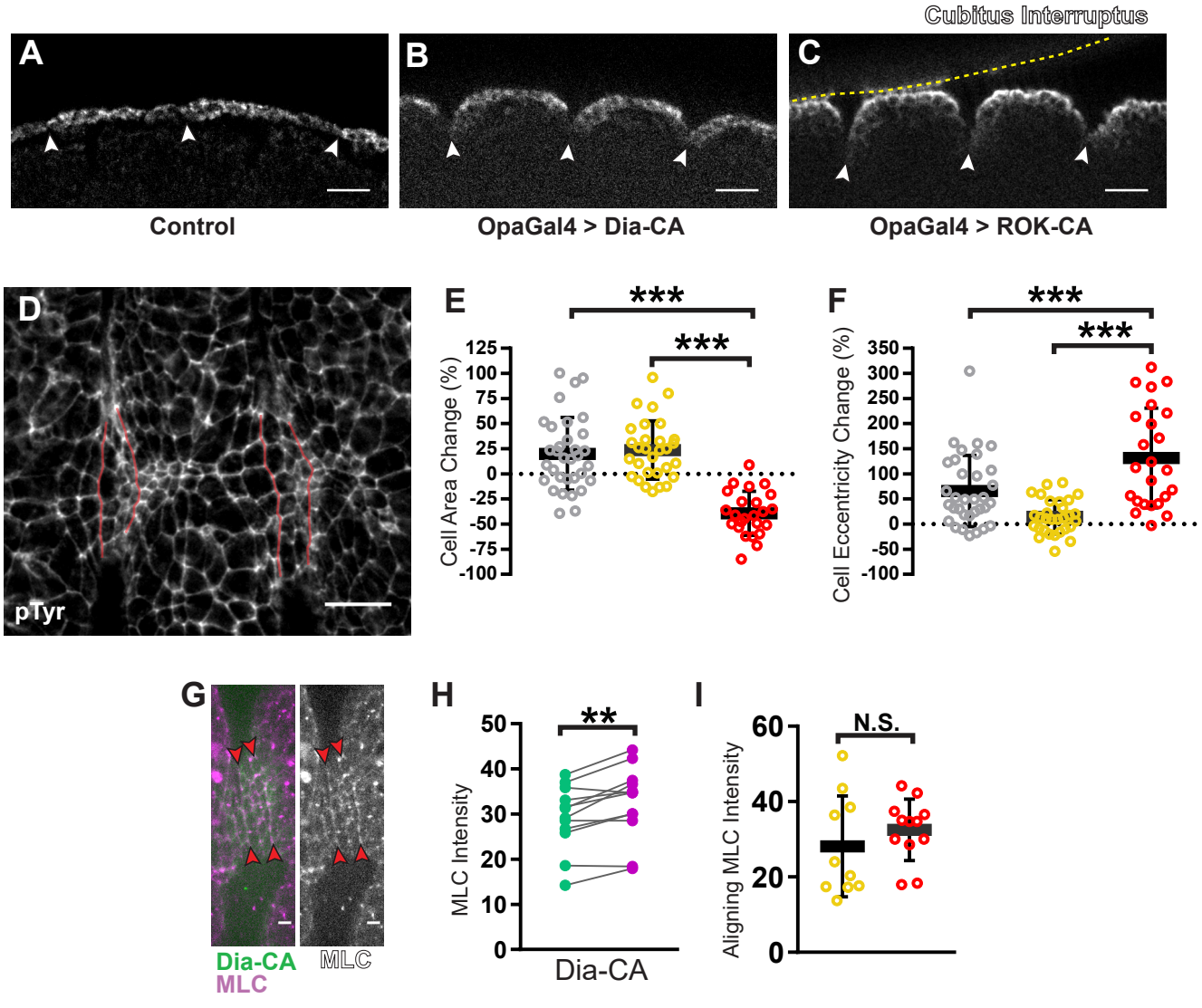

Figure S5. Constitutive activation of both Dia and ROK induces ectopic furrow formation.
(A-D) Ectopic furrows only form where aligning interfaces would normally form. (A) The boundary of Cubitus Interruptus expression is located at the anterior aligning interface (arrowheads). These regions are flat in wild type embryos. Upon expression of (B) Dia-CA or (C) ROK-CA with Opa-GAL4, ectopic furrows form at the Cubitus Interruptus boundary. Cross sections of the ventral epidermis are shown with the apical surface on top. Above the yellow dashes line, a second, irrelevant embryo lies in the field of view. CTRL: representative of 5 embryos; Dia-CA: representative of 4 embryos; ROK-CA: representative of 5 embryos

(D) ROK-CA expression results in additional cell morphology changes across the epithelium in addition to furrow formation. Red lines mark the aligning interfaces within the ectopic furrows. pTyr antibody staining marked cell outlines. Representative of 5 embryos

(E) Cell surface area significantly decreases upon Dia-CA expression (red) compared to adjacent, control interfaces (yellow) or to interfaces in wild type embryos (gray). WT: 33 cells, 4 embryos; Ctrl: 30 cells, 4 embryos; Dia-CA: 24 cells, 4 embryos

(F) Cell eccentricity significantly increases upon Dia-CA expression (red) compared to adjacent, control interfaces (yellow) or to interfaces in wild type embryos (gray). WT: 33 cells, 4 embryos; Ctrl: 30 cells, 4 embryos; Dia-CA: 24 cells, 4 embryos

(G-I) Dia-CA expression does not enhance or alter the planar polarized distribution of MLC at aligning interfaces. (G) Dia-CA::GFP (green) was expressed with Eve-GAL4 and MLC::mCherry (magenta) was imaged. (H) MLC was still significantly enriched at aligning junctions relative to orthogonal cell-cell contacts. Each line represents one interface and matches orthogonal (green) and aligning (purple) measurements. Orthogonal & Aligning: 12 interfaces, 7 embryos. (I) There was no significant difference in the amount of MLC at aligning junctions in Eve-GAL4 > Dia-CA expressing segments (red) in comparison to control segments (yellow). CTRL: 10 interfaces, 6 embryos; Dia-CA: 12 interfaces, 7 embryos

***$p<0.0001$, **$p<0.01$. (F) The Wilcoxon Rank paired test. (G) The Mann-Whitney U-test. Error bars = S.D. (A-D) Scale bars = 12μm, (E) Scale bars = 4 μm.

FIGURE S6

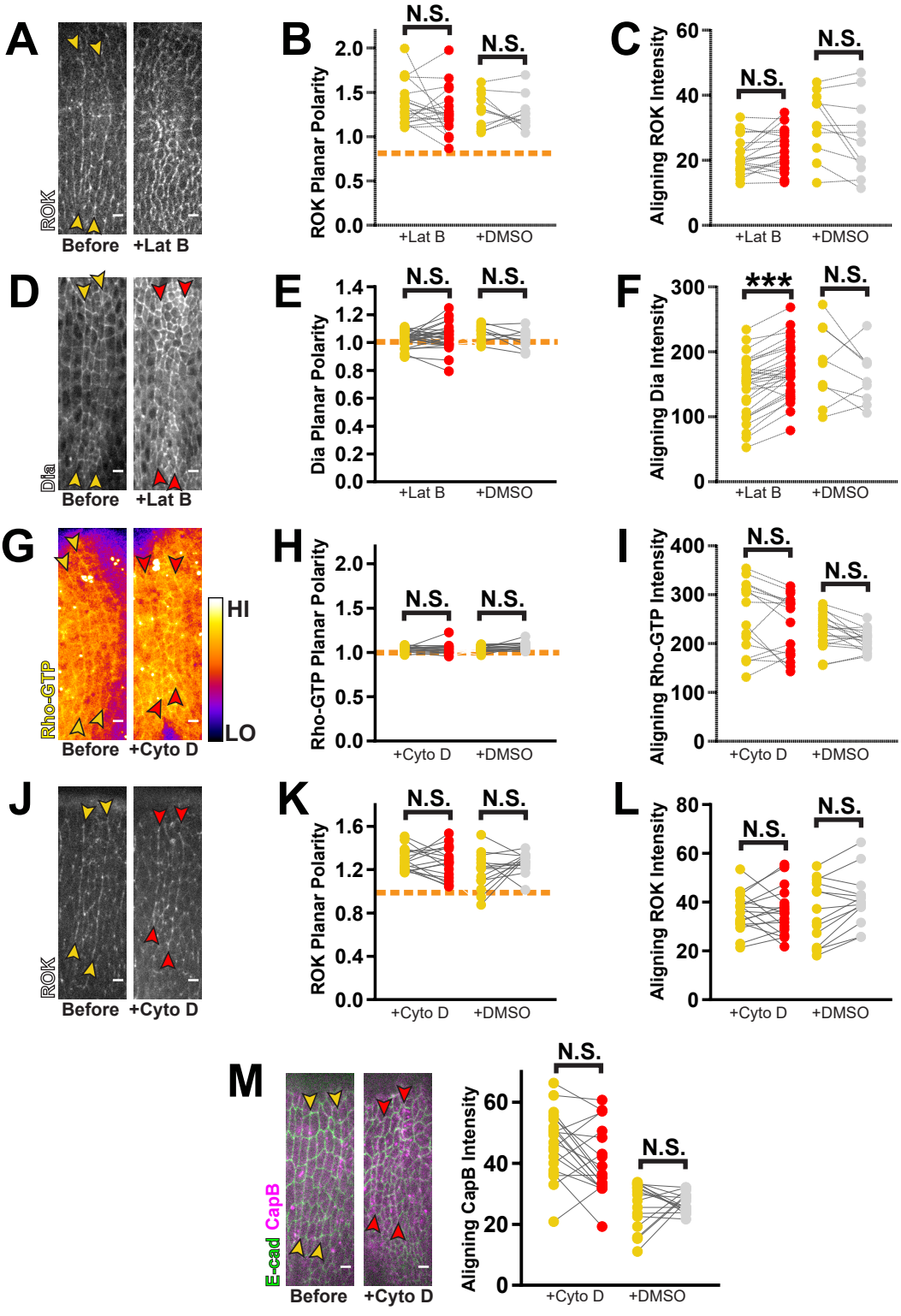

Figure S6. CytoD and LatB have different effects on Rho pathway components.

(A-C). LatB caused defects in ROK distribution along junctions. (A) GFP::ROK^{K116A} appeared more punctate at cell junctions after drug treatment. (B) Planar polarity and (C) the amount of ROK at aligning junctions did not change significantly with LatB treatment. LatB: 20 interfaces, 5 embryos; DMSO: 11 interfaces, 3 embryos

(D-F) Dia recruitment increases upon LatB treatment. (D) Dia::GFP was imaged, revealing the distribution of Dia at aligning interfaces before (yellow arrowheads) and after (red arrowheads) LatB treatment. (E) The planar polarized distribution of Dia was not affected by LatB exposure.

(F) The levels of Dia at aligning interfaces increased with drug treatment. LatB: 30 interfaces, 6 embryos; DMSO: 9 interfaces, 3 embryos

(G-I) CytoD does not alter Rho-GTP distribution. (G) Rho-GTP is visualized with a GFP-labelled sensor. Fluorescence intensity is displayed with the Fire LUT (calibration bar shows Low to High signal). Yellow arrowheads indicate interfaces before drug treatment and red arrowheads mark interfaces after CytoD injection. Neither (H) Rho-GTP planar polarity or (I) levels at aligning junctions changed significantly after CytoD treatment. CytoD: 16 interfaces, 6 embryos; DMSO: 18 interfaces, 5 embryos

(J-L) CytoD does not alter ROK distribution. (J) GFP::ROK^{K116A} was live imaged. Yellow arrowheads indicate interfaces before drug treatment and red arrowheads mark interfaces after CytoD injection. Neither ROK planar polarity (K) or levels at aligning junctions (L) changed significantly after CytoD treatment. CytoD: 18 interfaces, 5 embryos; DMSO: 8 interfaces, 3 embryos

(M) CytoD has no effect on CapB cortical levels. CapB::mCherry (magenta) was imaged with E-cad::GFP (green) as a reference for cell junctions. Yellow arrowheads indicate interfaces before drug treatment and red arrowheads mark interfaces after CytoD injection. CapB levels at aligning junctions did not change significantly with CytoD injection. CytoD: 20 interfaces, 6 embryos; DMSO: 16 interfaces, 4 embryos

Each line represents one interfaces and matches measurements before (yellow) and after (red) drug treatment or vehicle treatment (gray).

No significant changes in fluorescence intensity or planar polarity were observed with control injections of either 50% DMSO (for CytoD) or DMSO (for LatB).

***$p<0.0001$, (E,F) As explained in text, (D-F) the Wilcoxon-Rank test was used to assess statistical significance for changes. For all other experiments, the Mann-Whitney U-test was used. Scale bars = 4μm.

FIGURE S7

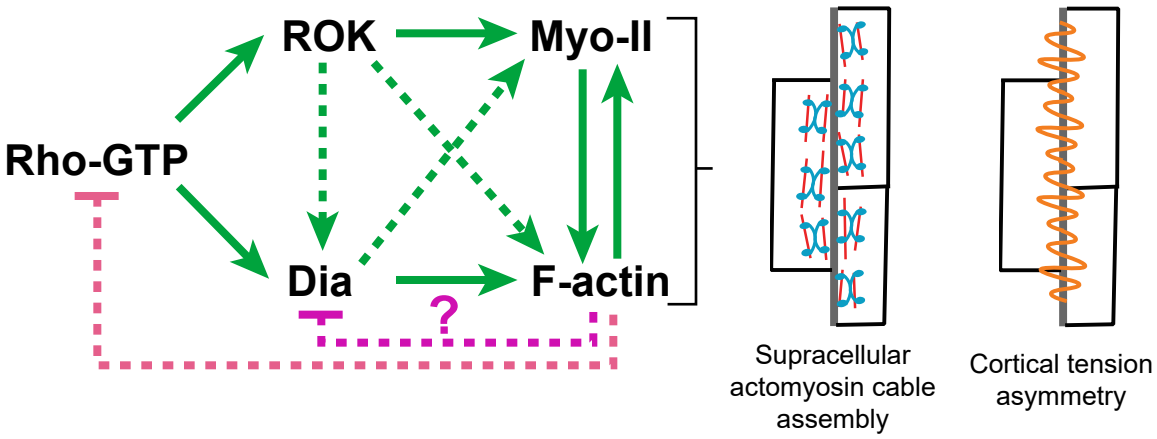

Figure S7. Model of Rho pathway interactions that mediate polarization of actmyosin assembly and cortical tension during alignment.

Green lines indicate positive regulation while pink/magenta lines indicate inhibitory interactions. Solid lines indicate direct interactions. Dashed lines signify interactions that may be indirect.

Table S1. Fly Stock and Reagent Sources

RESOURCE OR REAGENT	SOURCE	LOCATION	IDENTIFIER
Antibodies			
Mouse anti-phospho-Tyrosine (pTyr)	Millipore	Burlington, MA, USA	4G10 - Cat#05-321
Rabbit anti-Dia	Steven Wasserman	San Diego, CA, USA	(Afshar et al., 2000)
Rabbit anti-RFP	Abcam	Cambridge, United Kingdom	Cat# 62341
Chicken anti-GFP	Aves Labs	Tigard, OR, USA	GFP-2010
Rabbit anti-GFP	Invitrogen	Carlsbad, CA, USA	A-11122
Alexafluor Secondary Antibodies (488, 647)	Molecular Probes	Carlsbad, CA, USA	N/A
Cy3 Affinipure Secondary Antibodies	Jackson Immunoresearch Laboratories	West Grove, PA, USA	N/A
Chemicals			
Para-formaldehyde (PFA) 16%	Electron Microscopy Sciences	Hatfield, PA, USA	15710
PFA 40%	Electron Microscopy Sciences	Hatfield, PA, USA	15715-S
Rhodamine-conjugated Phalloidin	Invitrogen	Carlsbad, CA, USA	R415
Alexafluor 647-conjugated Phalloidin	Invitrogen	Carlsbad, CA, USA	A-22287
27 Weight halocarbon oil	Halocarbon Products Corp	River Edge, NJ, USA	9002-23-9
700 Weight halocarbon oil	Sigma Aldrich	St. Louis, MO, USA	H8898-100mL
Y-27632 dihydrochloride (ROK inhibitor)	Sigma Aldrich	St. Louis, MO, USA	Y0503
Latrunclin B	EMD Millipore	Burlington, MA, USA	428020-1MG
Cytochalasin D	Santa Cruz	Santa Cruz, CA, USA	201442
SMIFH2 Formin inhibitor	Sigma Aldrich	St. Louis, MO, USA	S4826-5MG
Propyl-gallate	Sigma Aldrich	St. Louis, MO, USA	P3130
Normal Donkey Serum (NDS)	Jackson Immunoresearch Laboratories	West Grove, PA, USA	017-000-121
Normal Goat Serum (NGS)	Jackson Immunoresearch Laboratories	West Grove, PA, USA	005-000-121
Hoescht	Sigma Aldrich	St. Louis, MO, USA	14530
Experimental Models			
w^{1118}	Bloomington Drosophila Stock Center (BDSC)	Marseille, France; Bloomington, IN, USA	BL#3605

Ubi::Ani-RBD-GFP; sqh-Moe-ABD::mCherry	Made with Ubi-Ani-RBD::GFP (gift from Thomas Lecuit) and sqh-Moe-ABD::mCherry (BDSC)	Marseille, France; Bloomington, IN, USA	(Munjal et al., 2015) and BL#35521
Ubi::Ani-RBD-GFP; Ubi-Par3::mCherry	Made from Ubi-Ani-RBD-GFP (gift from Thomas Lecuit) and Ubi-Par3::mCherry (gift from Yohannes Bellaiche)	Marseille, France; Paris, France	(Bardet et al., 2013; Munjal et al., 2015)
sqh^{AX3}; sqh-sqh::GFP	Gift from Roger Karess	Paris, France	(Royou et al.)
sqh^{AX3}; E-cad::tdTomato; sqh-sqh::GFP	Made with sqhAx3;sqh-sqh::GFP (gift from Roger Karess) and E-cad::tdtTom (gift from Yang Hong)	Paris, France; Pittsburgh, PA, USA	(Huang et al., 2009; Royou et al.)
UAS-Dia::GFP	BDSC	Bloomington, IN, USA	BL#56751
UAS-dia^{FH3FH1FH2}::EGFP/CyO	BDSC	Bloomington, IN, USA	BL#56753
Frl$^{MI03375\text{-}GFSTF.0}$/TM3, Sb^{1} Ser^{1}	BDSC	Bloomington, IN, USA	BL#60195
Capu$^{MI05737\text{-}GFSTF.0}$/CyO	BDSC	Bloomington, IN, USA	BL#66507
DAAM$^{MI04569\text{-}GFSTF.0}$ lncRNA:CR46248$^{MI04569\text{-}GFSTF.0\text{-}X}$/FM7j, B^{1}	BDSC	Bloomington, IN, USA	BL#60213
dia^{2}/CyO-Dfd-GMR-nvYFP	*dia*^{2} Gift from Steve Wasserman and BDSC	San Diego, CA, USA and Bloomington, IN, USA	(Castrillon and Wasserman, 1994) and BL#23230
rho1^{72O}/CyO-Dfd-GMR-nvYFP	BDSC	Bloomington, IN, USA	BL#7325 and BL#23230
rho1^{72F}/CyO-Dfd-GMR-nvYFP	BDSC	Bloomington, IN, USA	BL#7326 and BL#23230
UAS-Pav shRNA	BDSC	Bloomington, IN, USA	BL#42573
E-cad::tdTomato	Gift from Yang Hong	Pittsburgh, PA, USA	(Huang et al., 2009)
E-cad::tdTomato; Tubulin-GAL4	Made from E-cad::tdTomato (gift from Yang Hong) and Tubulin-Gal4 (BDSC)	Pittsburgh, PA; Bloomington, IN, USA	(Huang et al., 2009) BL#5138
Engrailed-GAL4, UAS-mCherry::NLS; UAS-DeGradFP/TM3,Sb	BDSC	Bloomington, IN, USA	BL#38420
sqh^{AX3}; sqh-Utr-ABD::GFP, sqh-sqh::mCherry	Gift from Adam Martin	Cambridge, MA, USA	(Mason et al., 2013)
sqh-GFP::ROK^{K116A}, Ubi-Par3::mCherry	Made from sqh-GFP::ROK^{K116A} (gift from Jennifer Zallen) and Ubi-Par3::mCherry (gift from Yohannes Bellaiche)	New York, NY, USA; Paris, France	(Bardet et al., 2013; Simoes et al., 2014)
E-cad::tdTomato; sqh-GFP::ROK^{K116A}	Made from E-cad::tdTomato (gift from Yang Hong) and sqh-GFP::ROK^{K116A} (gift from Jennifer Zallen)	Pittsburgh, PA; New York, NY, USA	(Huang et al., 2009; Simoes et al., 2014)

Ubi-E-cad::GFP, sqh-sqh::mCherry/CyO-Dfd-GMR-nvYFP	Made from Ubi-E-cad::GFP (gift from Jennifer Zallen), sqh-sqh::mCherry (gift from Adam Martin) and sna^{sco}/CyO-Dfd-GMR-nvYFP (BDSC)	New York, NY; Cambridge, MA; Bloomington	(Martin et al., 2009; Oda and Tsukita, 2001) BL#23230
Eve-GAL4	BDSC	Bloomington, IN, USA	BL#40732
Opa-GAL4	BDSC	Bloomington, IN, USA	BL#47406
E-cad::tdTomato; Eve-GAL4	Made from E-cad::tdTomato (gift from Yang Hong) and Eve-GAL4 (BDSC)	Pittsburgh, PA, USA and Bloomington, IN, USA	(Huang et al., 2009) and BL#40732
UAS-mCherry::NLS	Gift from Amin Ghabrial	New York, NY, USA	N/A
sqh-sqh^{WT}::GFP	Gift from Jennifer Zallen	New York, NY, USA	(Kasza et al., 2014)
sqh-sqh^{EE}::GFP	Gift from Jennifer Zallen	New York, NY, USA	(Kasza et al., 2014)
UAS-rok^{CA}::HA	Gift from Jennifer Zallen	New York, NY, USA	(Simoes et al., 2014)
Ubi-Ecad::GFP; tGPH	Made from Ubi::Ecad-GFP (gift from Jennifer Zallen) and tGPH (BDSC)	New York, NY, USA and Bloomington, IN, USA	(Oda and Tsukita, 2001) and BL#8164
Ubi-CPB::mCherry	BDSC	Bloomington, IN, USA	BL#58726
Software			
FIJI	www.fiji.sc	N/A	N/A
ImageJ	www.imagej.nih.gov/ij/	Bethesda, MD, USA	N/A
Metamorph Microscopy Automation and Image Analysis Software	Molecular Devices	San Jose, CA, USA	N/A
Axio-Vision Imaging Software	Zeiss	Oberkochen, Germany	Version 4.8
Graphpad Prism	Graphpad Software	San Diego, CA, USA	Version 7.00
Andor IQ3 Live Cell Imaging Software	Andor	Belfast, United Kingdom	N/A

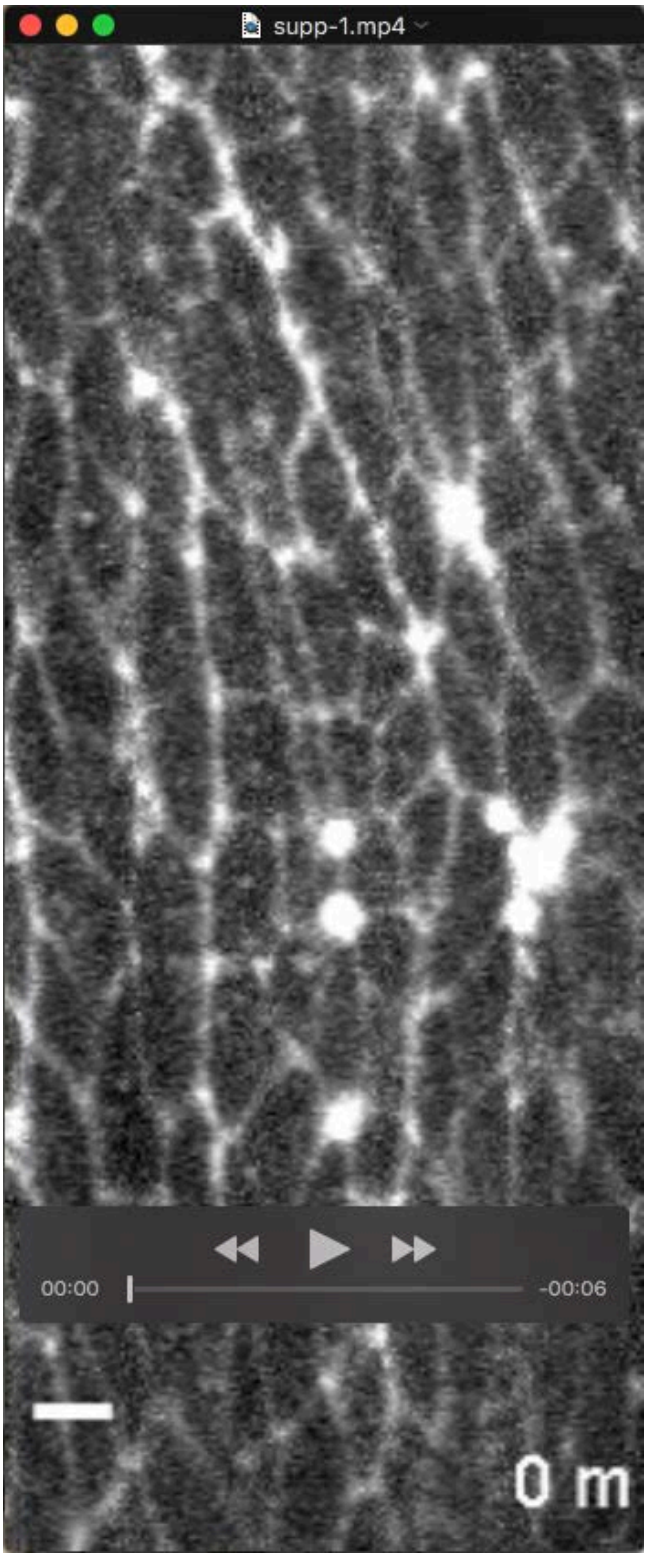

Movie 1. The effect of LatB treatment on F-actin distribution. Time point 0 shows the epithelium before drug treatment. F-actin is visualized with Utr-ABD::GFP. Scale bar = 4 µm. Representative of 4 embryos.

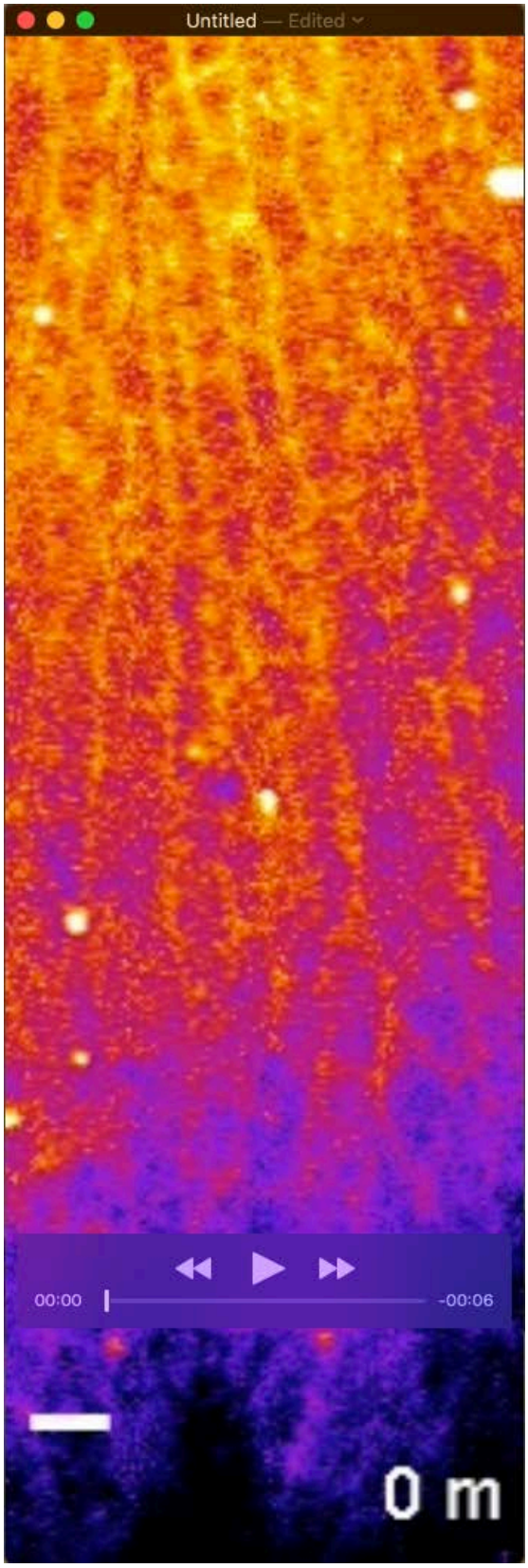

Movie 2. The effect of LatB treatment on Rho activation. Time point 0 shows the epithelium before drug treatment. GTP-bound Rho is visualized with the Rho sensor (Ubi-Ani-RGB::GFP). Scale bar = 4 µm. Representative of 4 embryos.

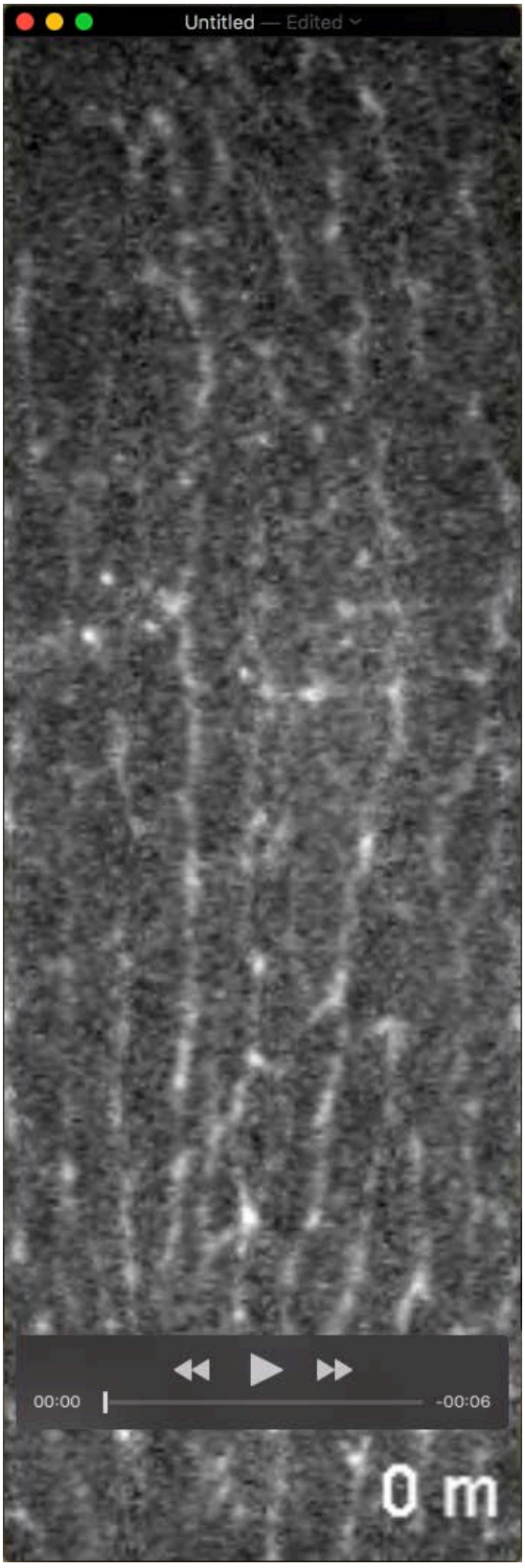

Movie 3. The effect of LatB treatment on ROK distribution. Time point 0 shows the epithelium before drug treatment. ROK localization is visualized with GFP::ROK^{K116A}. Scale bar = 4 µm. Representative of 5 embryos.

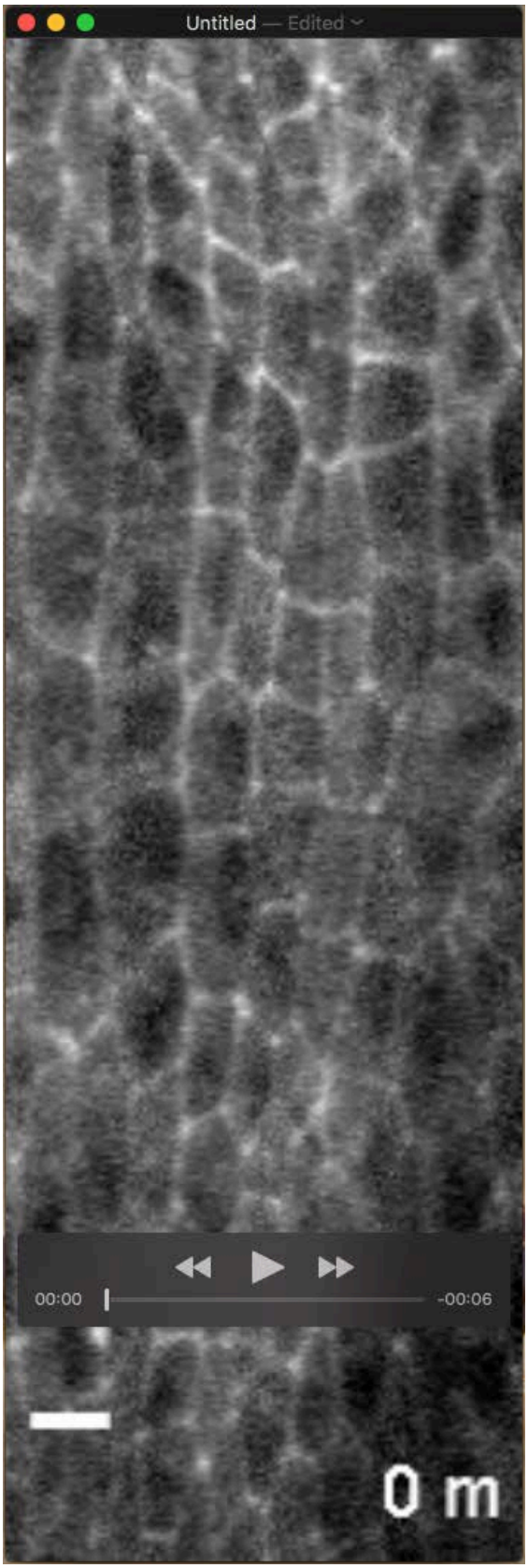

Movie 4. The effect of LatB treatment on Dia distribution. Time point 0 shows the epithelium before drug treatment. ROK localization is visualized with Dia::GFP. Scale bar = 4 μm. Representative of 6 embryos.

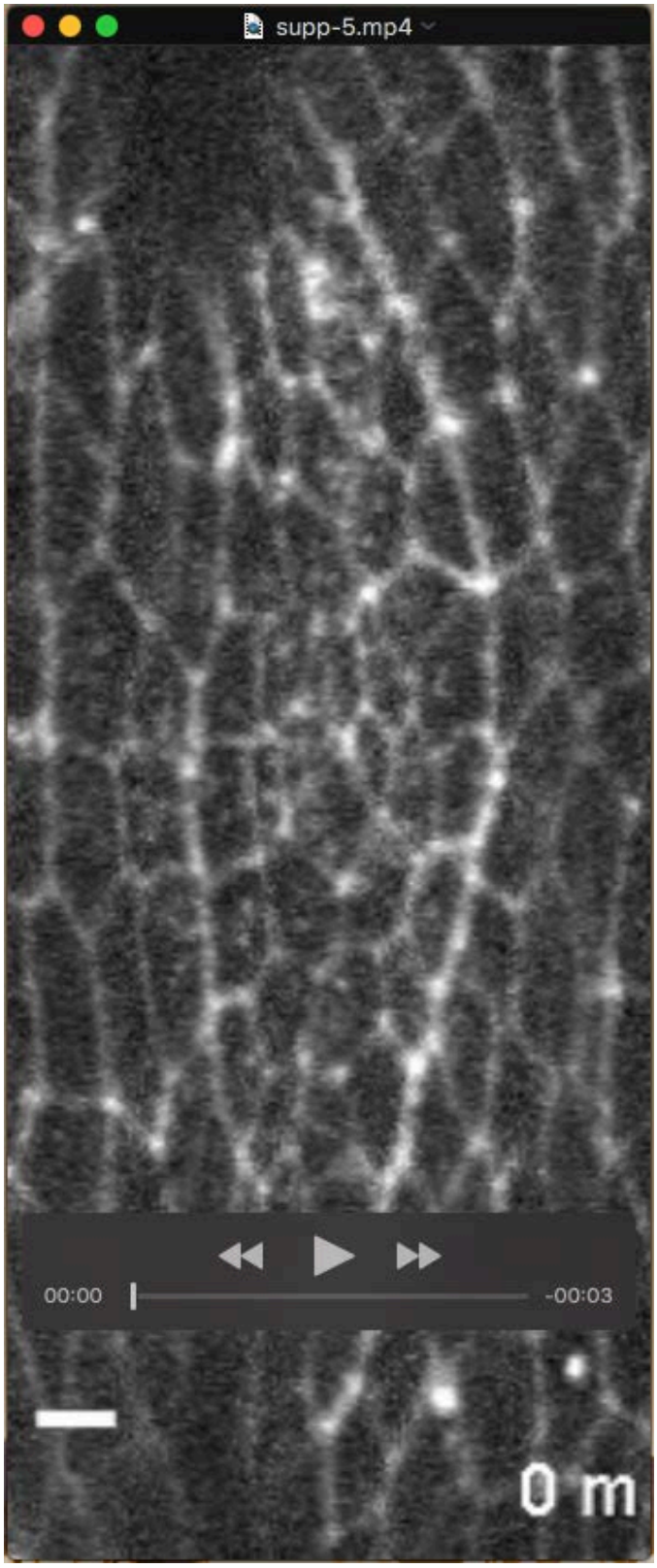

Movie 5. The effect of CytoD treatment on F-actin distribution. Time point 0 shows the epithelium before drug treatment. F-actin is visualized with Utr-ABD::GFP. Scale bar = 4 µm. Representative of 5 embryos.